Nanoscale

Accepted Manuscript

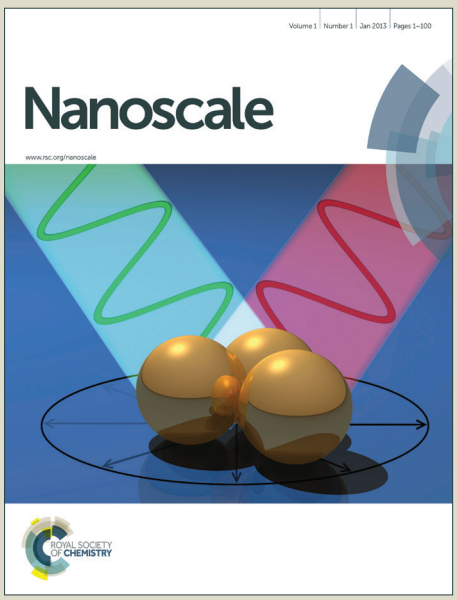

ROYAL SOCIETY OF CHEMISTRY

www.rsc.org/nanoscale

Nonlinear Current-Voltage Characteristics and Enhanced Negative Differential Conductance in Graphene Field Effect Transistors

Lin Wang*, Xiaoshuang Chen*, Yibin Hu, Anqi Yu, and Wei Lu

National Laboratory for Infrared Physics, Shanghai Institute of Technical Physics, Chinese Academy of Sciences, 500 Yutian Road, Shanghai 200083, China

Synergetic Innovation Center of Quantum Information & Quantum Physics, University of Science and Technology of China, Hefei, Anhui 230026, China

ABSTRACT: Recent observations of negative differential conductance (NDC) phenomenon in graphene field-effect transistors (FET) open up new opportunities for the applications of graphene-based fast switch, frequency multiplier and, most importantly, the high frequency oscillator up to the terahertz regime. Unlike the conventional two-terminal NDC devices, relying on the resonant tunneling and inter-valley transferring, in the present work, it has been shown that the universal NDC phenomenon of graphene-based FETs originates from their intrinsic nonlinear carrier transport under strong electric field. The operation of graphene-NDC device depends strongly on the interface between graphene and dielectric materials, scattering-limited carrier mobility, and saturation velocity. To reveal such NDC behavior, the output characteristics of GFET are investigated rigorously with both analytical model and self-consistent transport equation, multi-electrical parameter simulation. It is indicated that the contact-induced doping effect plays an important role in the operational efficiency of graphene-based NDC device, rather than the ambipolar behavior associated with the competition between electron and hole conductances. In the absence of NDC regime or beyond NDC one, the ambipolar transport begins at $V_{ds}>2V_{gs}$ at the drain end, it is exhibited that the kink-like saturation output characteristic is enhanced by the quantum capacitance contribution when the dielectric layer is thinning down. The observations reveal the intrinsic mechanism of NDC effect and open up new opportunities for the performance improvement of GFETs in future high-frequency applications beyond the paradigm based on two-terminal diodes.

KEYWORDS: negative differential conductance, graphene, field effect transistor, kink effect

Graphene has attracted extensive research interests recently due to its outstanding chemical, mechanical and electronic properties, and numerous potential applications[1-7]. Most of the interests in the graphene are based on its very high intrinsic carrier mobility in together with the ability to tune the carrier density in a wide range through field effect[8, 9]. The potential performance of graphene field effect transistors (GFETs) in radio frequency (RF) electronics is currently one of the hottest issues[10]. The cutoff frequencies f_T in GFET surpassing 300GHz has been reported and the further scaling into THz in sub-10nm channel has been predicted. Such results have demonstrated great promising for future applications[10,11-13]. However, due to the absence of bandgap in Dirac/chiral electronic band structure, the GFETs suffer from poor pinch-off and current saturation[14, 15]. The limitations could be a roadblock for their exploitation in RF electronics as the intrinsic voltage gain can be limited by the ratio $A_V=g_m/g_d$[14] (g_m is the transconductance and g_d is the derivative of the drain-current I_{ds} with respect to the drain voltage V_{ds}).

A weak saturation-like characteristics has been observed frequently in monolayer GFETs with further improvements of performance either by introducing a small bandgap in bilayer GFETs or optimizing the interface between the graphene and the dielectric layers[14,16,17]. Due to the ambipolar characteristic of graphene, the increase of drain bias can move the Dirac point into the channel, changing the conduction type near the drain-end from n-type (p-type) to p-type (n-type). The mechanism has been considered as the main reason for the saturation-like (or kink) behavior in the output characteristics, even for the recent observation of negative differential conductance (NDC) phenomenon in GFETs[16, 18, 19]. Intuitively, it is contrary that the NDC phenomena and current saturation can also be observed in backgated-GFET with only one type carrier injection from contact into the channel[20]. In addition, there are very few reports of GFETs that shows saturated behavior based on the phonon scattering under direct current (DC) measurement[17, 21]. The uncertainty and debate in the present experimental results needs more reliable characterizing techniques, in order to understand the intrinsic electrical properties and further performance optimization.

In this Letter, we examine the intrinsic electrical transport properties of GFET under high fields with the systematic studies including NDC, kink effects, velocity saturation, and potentially performance parameters for low output conductance g_d. The GFET devices studied here consist of three terminal top-gated structures (see Fig. 1(a)), where the top-gate extends over to the side contacts in order to minimize the access resistance. In the configuration, the gate voltage (V_{gs}) is used to modulate the density of graphene sheets with the source-contact being grounded, so that the ambipolar carrier transport begins when the chemical potential $\mu_{e,h}$ approaching the Dirac point at the drain end[18, 19]. Even though the substrates with high surface polar optical phonon (SPP) are desirable (e. g. silicon carbide (SiC) with $\hbar\omega_{spp}$~116meV[22]) for higher power and voltage gain[11], for simplicity, we suppose that the substrate-related effects are captured sufficiently. The results presented here are well suited to explore the desired performance of GFETs fabricated with either large-CVD[23] or SiC[19] graphene films.

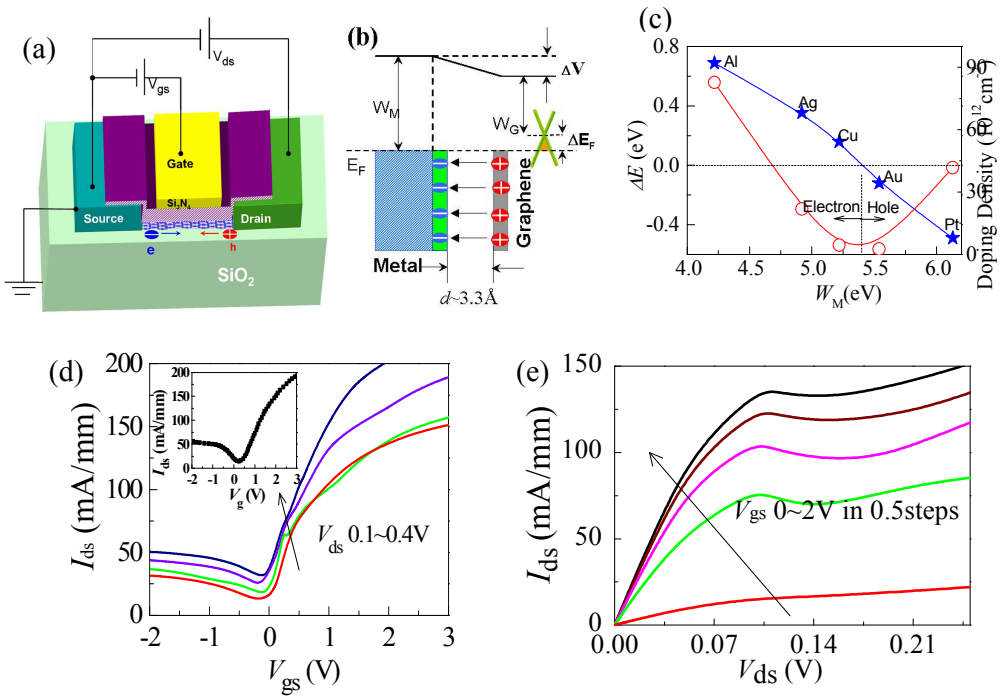

Figure 1. (a) Schematic of a three-terminal top-gated GFET, the thickness W_{IN} of Si_3N_4 dielectric layer is 20nm. (b)Schematic of dipole formation at the interface between graphene (work function W_G) and metal contacts (work function W_M), the equilibrium separation *d* between graphene and contacts is around 3.4Å. (c) The shift of Fermi energy (left axis and open circles) relative to the CNP (charge neutral point) due to the contributions of the chemical interaction between metal and graphene, and the work function difference W_M-W_G. Meanwhile, the metal-induced doping is also shown in the right axis with pentagon symbols, and the vertical dashed line distinguishes between the electron and hole doping regimes. (d)The transfer characteristic I_{ds}-V_{gs} of GFET under different drain bias V_{ds} is obtained through self-consistent transport equation and electrical parameter solutions (see Materials and Methods). Inset shows the experimental results from Ref. 19. (e)The output characteristics of GFET under different gate bias V_{gs}. The evolution of peaks and valleys can be observed clearly, indicating three transport regimes in the graphene NDC device.

In the previous reports, the mismatch of work-functions, between the graphene sheets and the source/drain contacts deposited by the e-beam evaporation, has been ignored. In fact, the metal-induced doping effect at the contacts depends on not only the electron transfer between metal and graphene, but also the strength of metal-graphene chemical interaction which plays an important role in dipole formation[23, 24], seeing Fig. 1(b) and discussions later. In a freestanding graphene, the Fermi energy coincides with the Dirac point. When graphene is chemisorbed on metal-contact, the graphene bands are perturbed and acquire a mixed graphene-metal character. However, the Dirac cone is not destroyed in the weaker interaction between graphene and metal, but instead shifts the Fermi level leading to the electron transfer from one to the other to equilibrate the Fermi level and the formation of interface dipole layer *d* (seeing Fig. 1b). Therefore, the potential step ΔV caused by the electric dipole consists of the "noninteracting" charge transfer Δ_{tr} driven by the difference W_d of the work functions (W_M-W_G), and Δ_c induced by chemical

interaction or the perturbation of atom-orbital. The "noninteracting" charge transfer Δ_{tr} can be modeled by parallel-plate capacitor model $\Delta_{tr}=C_e N d$, C_e is the capacitance of graphene unit-cell, $N\sim\xi\Delta E_F^2/2$ is the number of electron per unit-cell transferred from graphene to the metal. From Fig. 1b, the shift of Fermi level is modeled as $\Delta E_F=W_M-W_G-\Delta V$. In combination with the integrated electron number per unit cell, the Fermi energy shift ΔE_F with respect to the conical/Dirac point can be solved as[23]

$$\Delta E_F = \pm \frac{\sqrt{1 + 2C_e|W_d - \Delta_c|d} - 1}{C_e \xi d} \quad (1)$$

where the sign of ΔE_F is given by the sign of $W_d-\Delta_c$, as example, when considering Cu as metal contact, its work function is $W_M\sim5.22$eV, about 0.7eV (W_d) larger than that of graphene, due to the contribution of the chemical interaction term $\Delta_c\sim0.9$eV, Cu contact leads to the electron doping of graphene around$\sim4.47\times10^{12}$cm^{-2} rather than the hole doping predicted only by the electron transferring without chemical interaction. From Fig. 1c, it can be found that Au electrode has much weaker effects on the shift of Fermi level in graphene, therefore the band-bending or the flat-band voltage V_{FB} at the edge of contact is relatively small (see the following discussions). The results is also consistent with recent experimental results of C-V characterization[25], where the smaller contact resistance can be obtained in Au-graphene contact relative to other type of metals such as Cr or Ni which has stronger chemical interaction with graphene. The small contact resistance has been proved to be the result of minus band-bending near the edge of contact or the boundary between metal covered and uncovered graphene-channel. However, the band-bending depends obviously on the gate voltage and potential drop along the channel, and thus the contact resistance is in actually depends on the change of electric field, as shown in the following sections and experimental results in Ref. 25. Both the C-V and TLM results indicate that the contact resistance of Au electrode is increased significantly by sweeping the gate voltage to the n-type doping in corresponding to p-n junction formation at the boundary (see Fig. 1c), while the contact resistance reduces when the channel is p-type doped in corresponding to the overbarrier tunneling.

Such intrinsic electron or hole doping by contacts leads to the misalignment of charge neutral point (CNP) between contacts and channels, and thus the imbalance injection or conductance asymmetry is formed (e. g. Fig. 1(d)) between electron and hole branch. And ultimately the hole conduction branch is suppressed, as shown in Fig. 1(d) (Cu contact is used), in consistent with recent observations experimentally[26, 27]. In the meantime, the change of contact resistance would inevitably lead to redistribution of the electric field along the channel and thus play an important role on the high-field characteristic of current output as being found in the following discussions. Even though the chiral tunneling relevant NDC phenomenon has been predicted theoretically[28], the carrier dynamics investigated in our Letters are in the quasi-equilibrium diffusive transport regime (see Materials and Methods). Here, the effects mentioned above are implemented self-consistently with the well developed high-field electron-phonon scattering model. While other effects such as lattice-heating or the hot-electron-lattice nonequilibrium heat-transferring process are taken into account in the Supplementary Informations. Accordingly, our results are found in good agreement with that reported in recent experiments (inset of Fig. 1d). The results indicate that electrons are transferring from the metal-contact to the graphene sheet, which is also in well agreement with the predicted results in Fig. 1c. Most interestingly, the non-monotonous growth of the electron branch can be observed in the I_d-V_g characteristic (Fig. 1d), which is sharply different

from the hole branch. The NDC effect from such non-monotonous current-growth may have important applications for high-frequency oscillators. Beyond the NDC region, the I_d-V_d characteristics enter or recover into the sub-linear range (Fig. 1e). Although the NDC phenomenon has been predicted to be enhanced with smaller minimum conductivity σ_{min} (seeing the Supplementary Information) and without velocity saturation, it still lacks of reliable evidence on the fact that NDC is caused by the replacement of electron-dominated channel with hole-dominated one. Also it lacks of evidence why such effect can be observed at hole-branch of I_d-V_g characteristic when the drain bias is sufficient large[19]. Therefore, it is very necessary to perform self-consistent investigation of GFET's electrical properties by taking into account various potential mechanisms, such as velocity saturation effects, contact-induced electron-hole asymmetry etc. (see Materials and Methods), which are also the central points in our study.

In previous works, the NDC phenomenon has been observed frequently in conventional GaN or GaAs high electron mobility transistors due to the self-heating or hot electron effects (seeing Supplementary Information). While in our investigated regime, both of these effects are not strong enough to cause either the significant heating of electrons and lattice or the full-saturation of current output. Therefore, the NDC of graphene FETs is with the advantage of low threshold voltage driven due to the absence of bandgap. The quasi-Fermi level distribution (Fig.2a) along the channel is obtained under non-equilibrium carrier statistics, which is more rigorous than the surface potential analytical model derived in the diffusive transport limits[18]. Various physical quantities intimate to the output current are shown in Fig. 2 at four drain bias points, marked as 1, 2, 3, 4 by the arrows in the inset of Fig. 2(a). In contrast to the prediction in previous works[19, 29], the quasi-Fermi levels (E_{Fn}, E_{Fp}, E_{Fp}>E_{Fn} because of the n-type electrostatic doping) at the drain end are retaining above the Dirac points even when the device enters into the NDC regime. The sheet electron densities along the channel scale almost linearly with the drain bias V_{ds} due to the shift of the Dirac point presented in Fig. 1d. The behavior indicates relatively weak quantum-capacitance contribution. Before our going on, it should be noted that the total gate capacitance C_g can be modeled as a series connection between dielectric capacitance C_d and quantum capacitance C_q[18]:

$$C_g^{-1} = C_q^{-1}(\mu_{e,h}) + C_d^{-1} \qquad (2)$$

where the dielectric capacitance of Si_3N_4 (20nm) is C_d~0.3μF/cm^2, and the quantum capacitance C_q of graphene depends on the channel potential $\mu_{e,h}$~0.05eV,

$$C_q = \frac{2q^2kT}{\pi(\hbar v_F)^2}\ln\{2[1+\cosh\frac{\mu_{e,h}}{kT}]\}\text{, } v_F \text{ is the Fermi velocity} \qquad (3)$$

which is around 1.5μF/cm^2 in the NDC regime, five times larger than the dielectric capacitance C_d. Therefore, the dielectric capacitance rather than the quantum capacitance dominates the electrostatic doping efficiency in Fig. 2a. Specifically, the density-limited explanation (or the competition between electron and hole conductions) of NDC alone does not provide insight physical basis for developing graphene-based high-frequency mixers or oscillators.

In close to the drain end, the electronic drift velocity does not reach full saturation under the acceleration of electric field, instead of that, it is inert to the change of drain bias when the device

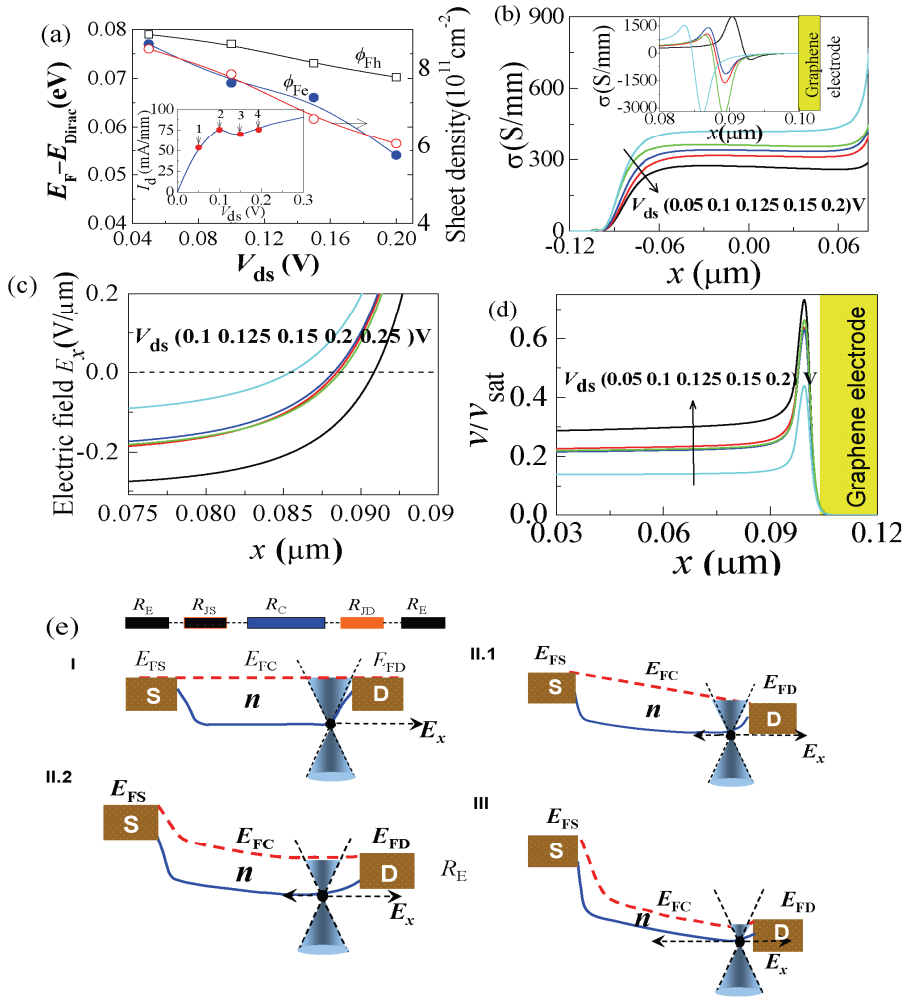

Fig. 2. (a) The variation of the quasi-Fermi level relative to the Dirac point (left axis) at four drain bias voltage points indicated in the inset (1-linear region, 2-peak region, 3-valley region, 4-sublinear region), the gate voltage is 0.5V, and the sheet density scales almost linearly when the drain bias V_{ds} is swept, right axis. (b) The local conductance distribution along the channel, with the drain bias changing from 0.05V to 0.2V. (c)The profile of self-consistent electric field along the channel, the dashed line denotes the flat-band region near the drain end, caused by the doping effect of metal-contact. (d) The change of electron velocity normalized to saturation velocity v_{sat} along the channel under different drain bias voltages. (e) Band diagram schematics of the graphene channel at gate voltage 0.5V. I, linear region, II NDC region with II.1 indicating that the junction resistance increases at source R_{JS}, and the junction resistance at drain R_{JD} is starting to drops, and II.2 Implying that - the output current characteristic returns to the sublinear region when the junction resistance R_{JD} at drain is reduced significantly. III. The sublinear regime of output current characteristic. The shaded regions of (b) and (d) indicate the locations of graphene electrodes.

enters into the NDC region. Meanwhile, the transverse electric field E_x along the channel remain

almost unchanged, owing to the pinning of Fermi level in the channel, seeing also the solid symbols in Fig. 2a. In order to understand better the intriguing phenomenon of electronic blocking, the conductance profile ($\sigma(x)=J(x)/E_x$) along the channel is displayed in Fig. 2b (with amplified view of conductance near the drain side in the inset). In apparently different from previous published works, we can clearly that the conductance has its opposite signs near the drain end (shaded region). This is mainly caused by the electrostatic screening of Fermi-level pining and band bending at the interface between metal-covered and uncovered graphene channels, and it has not yet been taken into account before. Besides, near the drain end, the electric field changes its direction so that the electrons experience deceleration in the negative conductance region. Furthermore, only the conductance around the drain end varies non-monotonously with the change of drain bias. Therefore, the blocking of carriers at this region plays the dominant role in the NDC effect of the overall I_d-V_{ds} characteristic. Since such conduction phenomenon is difficulty to be explained only through the simple analytical model without using the local electrical parameters obtained self-consistently[18,19], the actual mechanism of NDC effect may be concealed by using only ambipolar carrier transport instinctively. By the comparison of Figs. 2a and 2d, it can be found that the total current is mainly limited by the nonlinear increment of electron velocity or its saturation properties, rather than by the sheet density decrement alone (also seeing Materials and Methods). Thus, the NDC effect is mainly induced by the intrinsic high-field transport property of carriers in the graphene sheet, however, the effect is not always being observed during the experiments.

Generally, the output characteristic of GFET can be divided into three distinctive regions, I-the linear region, II-NDC region, and III-the sub-linear region (seeing Fig. 2e). From above discussions, it is known that three parasitic parameters dominate the output characteristic, the junction resistance $R_{JS,D}$ caused by the band-bending at the boundary between metal-covered and uncovered graphene channels, channel resistance R_C and contact resistance R_E. In the linear region I (Fig. 2e-I), the channel resistance R_C is nearly constant with voltage dropping across the channel or negative electric field E_x increasing monotonously. On the contrary, the junction resistance R_{JD} and R_{JS} near the interface between source or drain electrode and channel is not a constant (seeing Fig. 2b and Fig. 2e-II.1 and II.2) due to the strong field and density dependence of electron velocity or relaxation time[30]. Furthermore, the results indicate that the junction resistance R_{JS} near source is larger than R_{JD} when the drain bias increases. When the sheet density drops faster than the velocity at the drain end (i. e. the *condition 1* in Materials and Methods is satisfied)[29], the current output is reduced, and the device can inevitably enters the NDC regime (Fig. 2e-II). To maintain the negative electric field (E_x), the Fermi level should move closer to the Dirac point at the interface between channel and source or drain electrode of graphene (from Figs. 2e-II.1 to II.2) until the junction resistance R_{JD} at the drain side is sufficient low because the Fermi level E_{FD} is closer to the Dirac point than the Fermi level E_{FS}. To that end, when the voltage drop across the channel is increased again, the junction resistance at the drain (R_{JD}) is reduced further. Then, the sub-linear output characteristic is caused. As in the case of Fig. 2e-III, the Fermi level E_{FD} is very close to the Dirac point, and R_{JD} can be neglected. Thus, the NDC effect of output characteristic occurs prior to the ambipolar carrier transport regime. Our results also can be agreement with the recent observation of the NDC phenomenon in the back-gated GFET with only p-type carriers contributing to the differential conductance[20].

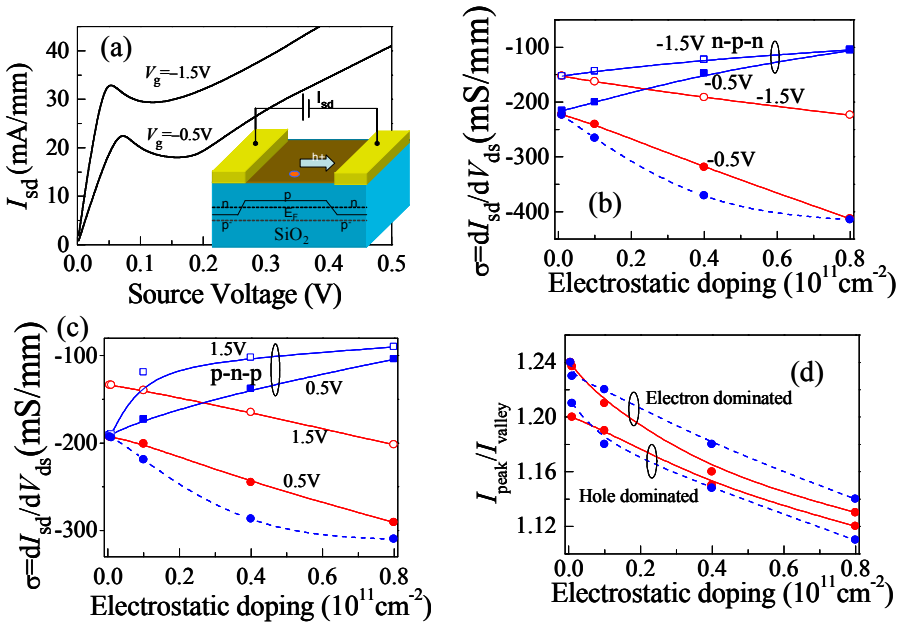

Fig. 3. (a) Output characteristics of GFET under the configuration of hole-conduction regime, with gate voltages V_g=−0.5V, −1.5V, inset indicates the induced p-n, p'-p junction at the contacts. (b) is the differential conductance of hole dominated device with different gate voltages depicted aside the curves, open and solid squares are n-type metal-covered graphene channel, and open and solid circles are p-type metal-covered graphene channel. (c) is the differential conductance of electron dominated GFETs as a function of electrostatic doping efficiency, solid and open squares are the p-type metal-covered graphene, and solid and open circles are n-type metal-covered graphene, the results with asymmetrical metal-stack used are shown by blue dashed lines with solid circles in (b) and (c). (d) are the peak to valley ratio of output current in hole and electron-dominated GFETs at 0.5V (solid lines) and 1.5V (dashed lines).

To indicate more clearly, Fig. 3(a) plots the output characteristic of GFET which is dominated only by the holes conduction in all bias ranges. As mentioned in above sections, it is possible that the electron transferring process between contacts and graphene will lead to the formation of two back to back, light doped n'-p junctions (e. g. Cu contacts, the inset of Fig. 3(a)) and depending on the type of metal stacks used. One can see from Fig. 3 that for the hole-dominated channel, the strength of NDC is more pronounced than the electron-dominated one, and depends strongly on the metal-induced electrostatic doping efficiency (Figs. 3(c) and (d)). Furthermore, it is interesting to see that metal-induced hole-doping will improve the strength of NDC, such results further demonstrate the essential role of carrier dynamics near the contacts. The hole-doping regime can be easily realized by using the metal contacts with larger work-functions such as Au, Pt etc. In Figs.3(b) and (c), the NDC increases along with the increasing of doping densities, but it should be noted that the in our discussed regime the screening length which controls the p-n junction width is around $l_s \sim 4\varepsilon_{oxide}\hbar v_F/(q^4\pi n_M)^{0.5}$~50nm. The induced-potential barrier near the interface between graphene channel and contacts is too long to cause ideal Klein transmission[31]. Without considering about the scattering of disorder in graphene channel, the conductance of graphene channel can be approximate as

$$g = g_0 \int_0^{|v|} \frac{\mathbf{T}_S \mathbf{T}_D \, d\kappa}{1-(1-\mathbf{T}_S)(1-\mathbf{T}_D)} \tag{4}$$

where g_0 is a constant, $T_{S,D}$ is Klein transmission or the overbarrier transmission at the source and drain, κ is the wavevector along the width direction, v is the gate voltage. Both the transmission at source (overbarrier) and drain (Klein) is increasing monotonously in the NDC region, therefore, only the junction resistance caused by the band-bending and depletion of carriers near the interface between metal-covered and uncovered channels affect the overall current-voltage characteristic. Therefore, in the diffusive regime and sufficient-high electric-field, the junction resistance in combination with the channel resistance would lead to the nonlinear dependence of current on the voltage as depicted in Fig. 2. In both of Figs. 3(b) and (c), the NDC effect is maximized when the asymmetrical metal contacts such as Cu and Au at opposite ends of GFET is used (e. g. for hole-dominated one, the Cu and Au cause lightly n and p type doping at drain and source of GFET, respectively). Therefore the physics of contact can have a significant effect on the transport properties of graphene. This also reminds us about the large variability of the NDC effect as observed in experiments, since the strength of the effect depends on the junction properties at the boundary between metal contact covered and uncovered regions of graphene channel, the kink-like effect (which would be discussed below) instead of the NDC effect is always being observed in Cr/Au contacted device due to the strong chemical interaction between the graphene and metal[16, 17], while the effect can take places in both back-gated and top-gated graphene FET with Pd or Au contacted graphene sheet[19, 20].

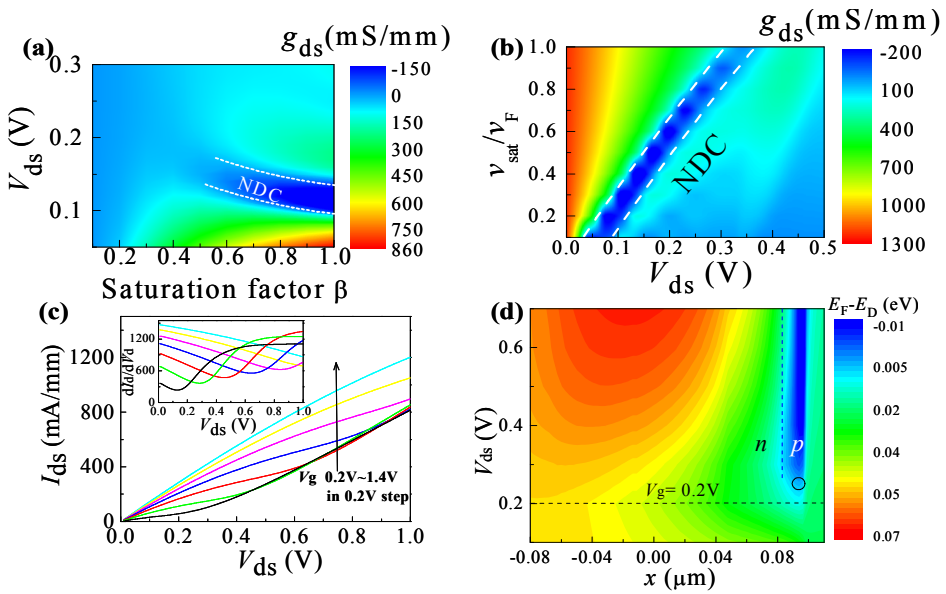

Fig. 4. (a) The color panel of output conductance g_{ds} with changing the saturation factor β and the drain bias. The NDC region is indicated by the dotted lines in dark-blue region. The kink-like behavior is visible at smaller saturation factor, related to the weaker scattering-limited mobility. (b) The dependence of output conductance on the saturation velocity v_{sat} depending strongly on the substrate, described with $v_{sat}=v_F(\hbar\omega_{OP}/E_F)$, $\hbar\omega_{OP}$ is the SPP phonon energy. (c) The output I_{ds}-V_{ds} characteristic under the different gate voltages when the device suffers from weaker phonon-scattering. Inset displays the corresponding output conductance, all the curves exhibit 'V'

shapes, and the minimum conductance exhibits obvious shift with different gate bias voltage. (d) The color map of difference between Fermi level and Dirac point distribution along the channel with the V_{gs}=0.2V. Hole-dominated transport is recognizable at the drain bias V_{ds} being larger than $2V_{gs}$.

Above all, the NDC phenomenon is the representative of the nonlinear carrier transport behavior in the graphene channel. However, when the carrier mobility depends relatively weakly on the density and electric field, or the saturation velocity v_{sat} is very high (see Materials and Methods), the output I_{ds}-V_{ds} characteristic should possibly exhibit slow saturation behavior. As shown in the previous reports, the drift velocity as a function of transverse electric field is accurately modeled by Thornber's equation[17, 32]

$$v_{\mathbf{drift}} = \left(\left(\frac{1}{\mu E_x} \right)^{\beta} + \left(\frac{1}{v_{\mathbf{sat}}} \right)^{\beta} \right)^{-1/\beta} \tag{5}$$

Fig. 4a shows a color plot of output conductance with changing the drain bias V_{ds} under different saturation factor β. Here, the physical meaning of β describes the field dependent scattering rate γ of optical and acoustic phonons, and the scattering rate γ is in proportional to the Fröhlich coupling constant $F_{\gamma}^{2} = \left[\frac{\mathrm{h}\,\omega_{\mathbf{SPP}}}{2\pi} \right] \left(\frac{1}{\varepsilon_{\infty} + \varepsilon_{\mathbf{env}}} - \frac{1}{\varepsilon_{0} + \varepsilon_{\mathbf{env}}} \right)$ ($\hbar\omega_{spp}$ is the surface polar optical phonon energy of the substrate), from where it can be predicted that $\gamma_{HfO2}>\gamma_{SiO2}>\gamma_{SiC}$ or $\beta_{HfO2}>\beta_{SiO2}>\beta_{SiC}$ and much stronger NDC can be observed in HfO_2 and SiO_2 dielectric structure[33, 34]. The main observation is that the NDC effect is replaced by the kink-like behavior when the saturation factor β is smaller than 0.6 and meanwhile the drain voltage is shifted upwards. It should be noted that the NDC effect in GFET can not always be observed from the experiments[14,16-18]. The reason is probably in relevant with the substrate-induced scattering effect except for the contact-induced doping mentioned above. In addition to the scattering rate γ, the high-field saturation velocity v_{sat} depends strongly on the energy of surface polar optical phonon mode. When the Fermi-level approaches to the Dirac point or the small bias voltage is applied, the saturation velocity v_{sat} is comparable to the Fermi velocity v_F[16]. The slow saturation behavior can be caused, as shown in Fig. 4b. Such results are in good agreement with the recent observation that the NDC effect is indicated under higher gate bias[18]. But it should be noted that the saturation velocity v_{sat} depends relatively weakly on the sheet density ($v_{sat} \propto n_s^{-0.5}$) due to the chiral electronic spectrum, and it varies only three times when the density changes from 10^{12} to 10^{13}cm^{-2}. In such case, other mechanism for the observation of NDC at higher gate bias would be the interplay between junction resistance $R_{JD,S}$ increment and density-limited output-current dropping at higher electrostatic doping, mentioned above.

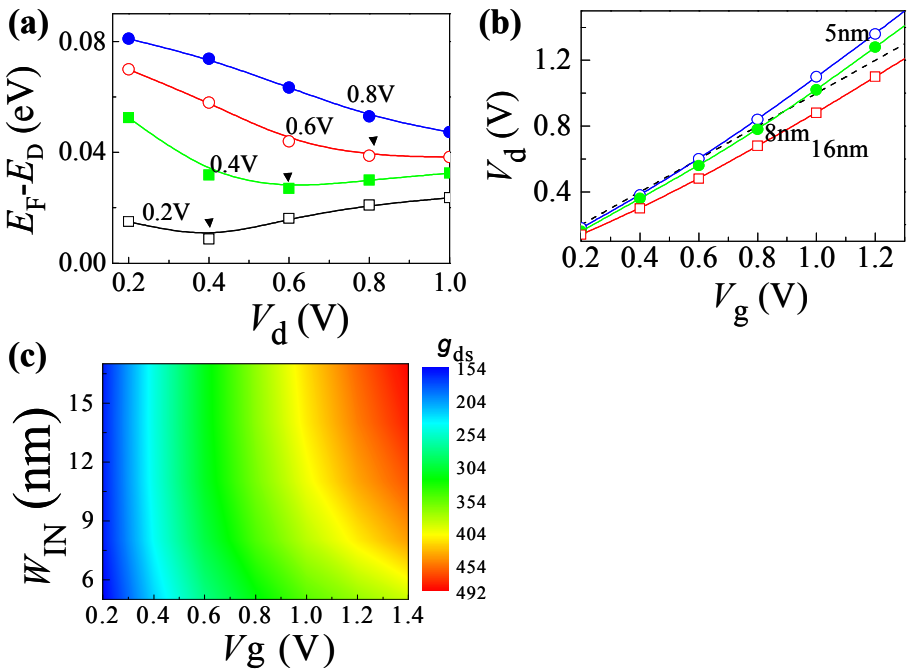

Figure 5. (a) The difference between Fermi level and Dirac point cutting at vertical dashed line in Fig. 3d under different gate and drain bias voltages. The non-monotonous V_d dependence of E_F-E_D is observed in the data, and the bias point of minimum difference between E_F and E_D marked by solid triangles shifts along the change of drain bias. (b) The dependence of minimum output conductance on the thickness of dielectric layer separating the gate from the graphene channel, and the gate and drain bias voltages. The dashed line denoting V_{gs}=V_{ds} is guiding to the eye. Larger drain bias is needed in order to move the Dirac point into the channel of GFET with thinner dielectric layer due to the larger quantum capacitance contributions. In addition, such behavior demonstrates the expansion of 'V' conductance distribution. (c) The dependence of minimum conductance on the gate voltage and thickness of dielectric layer. It can be seen that the saturation performance can be improved through thinning down the dielectric layer.

We have explained the NDC effect by considering the carrier saturation velocity behavior. Next, we seek to explore the kink-like behavior displayed in Fig. 4c. It is well known that such kink-like behavior has been observed frequently in the experiments[16-18]. In different from the results presented in Fig. 1e, all the curves are found to have a plateau, corresponding to the conductance minimum in the inset. Besides, the positions of conductance minimum in the curves are very close to the drain bias voltages. To visualize better, the panel of Fig. 4d depicts the change of Fermi energy relative to the Dirac point along the graphene channel with changing V_{ds}. When the drain bias is very close to the gate voltage V_{gs}, the polarity of channel at the drain end is actually unchanged, seeing the horizontal dashed line in Fig. 4d, and the conductance minimum or the pseudo-saturation usually happens before the Dirac point moves into the channel. The observation is in well consistent with the prediction of Ref. 16. The hole-dominated transport begins at the drain side when the drain bias V_{ds}>V_g, as shown in Fig. 4d with the black circles, and then the device recovers to the superlinear output characteristic due to the ambipolar carrier transport, as shown in the inset of Fig. 4c. It should be noted that the voltage difference $\Delta V \sim V_g -$

V_{ds} in the kink regime of output characteristic increases when the gate voltage increases. This is because when the drain bias V_{ds} approaches to the gate voltage V_g, the hole density n_{sh} is still far less than the electron one n_{se} at the drain side, in corresponding to the n^+-p junction. The hole density n_{sh} approaches to the electron density n_{se} when $V_{ds}>2V_g$, and then the Dirac point is caused to move into the channel when $n_{sh}>> n_{se}$ at the drain end. In the Fig. 5a, with the data being cut at the position, shown in the vertical dashed line in Fig. 4d, the non-monotonous change of Fermi level relative to the Dirac point indicates that larger portion of the drain voltage drops across the junction resistance localized at the drain side due to hole dominated transport, as confirmed also in Ref. 29 by KPFM methods. Even though the current saturation can be improved by introducing the band gap in bilayer graphene or graphene nano-ribbon, it is interesting that the saturation strength in GFET rely on not only the ambipolar transport, but also the thickness of dielectric layer. We find that minimum output conductance g_{ds} decreases with reducing the dielectric layer thickness W_{IN}. The result indicates that the better current saturation can be obtained, as shown in Fig. 5c. Such phenomenon can be understood by taking into account the effect of quantum capacitance C_q which dominates the total gate capacitance when $C_q<<C_d$ (seeing Eq. 2). The channel potential $V_{ch}(V_{ds}\sim 0)=V_gC_d/(C_d+C_q)$ increases when the Fermi level moves closer to the Dirac point (seeing Eq. 3). Meanwhile, the drain bias voltages have to be increased in order to overcome the potential increment caused by the quantum capacitance at the drain end, seeing Fig. 5b. When the Fermi level approaches to the Dirac point at the drain end, the low DOS (density of state) limits the carrier occupation especially for the device with larger quantum-capacitance contribution. The limitation leads to much improved saturation behavior, as shown in Fig. 5c. In addition, other parameters, such as the saturation velocity, mobility and doping level at the contact, also have an important role in the improvement of current saturation. Thus, one makes inevitably the trade-off in choosing interface-materials for achieving the high-power output and the best current saturation (seeing Materials and Methods).

In summary, the output characteristics of GFET in the diffusive transport limit are investigated rigorously by taking full advantage of self-consistent transport equation and electrical parameters. Our results demonstrate that the NDC effect caused by the density-limited nonlinear velocity saturation can be in principle applicable to all graphene materials. But it should be noted that such effect is not exclusive to the transport regime in this Letter, the chiral tunneling related-effect is also predicted in ballistic device[28]. To demonstrate the universality of such NDC phenomenon, the factors, such as mobility-decrement by high-field scattering events and local charge-density profile, are considered. The results indicate that the movement of Dirac point into the channel is not the prerequisite condition for the onset of NDC, instead, it could be an important condition to achieve the low output conductance of GFETs with zero band gap.

For the observability of the NDC effect in the realistic device, several parameters should be optimized, such as the choice of combination between top-gate dielectric and graphene with high interface quality, and the metal-contact doping-induced junction resistance R_J. It is predicted that the contacts may play a key role in determine the depth of the NDC regime. Here, the depth is approximately equal to I_{peak}/I_{valley}, as an example, the hole doping induced by the contacts can enhance the depth due to the increase of R_J at the interface between electrode and graphene channel. Our results also demonstrate that the onset of NDC is strongly dominated by the scattering-limited velocity saturation. Therefore, the magnitudes of mobility-decrement at the high-field and the SPP-scattering limited saturation velocity are important for the reproducible of

graphene-based NDC device. Otherwise, they both have detrimental effects on the NDC by narrowing the NDC operation window. In the absence of NDC regime or beyond NDC one, the ambipolar transport begins when $V_{ds}>2V_{gs}$ at the drain end, and the kink-like output characteristic is enhanced by the quantum capacitance contribution when the dielectric layer is thinning down. The observations reveal the potential mechanism for the NDC effect and open up new opportunities for the performance improvement of GFETs in future high-frequency application beyond the paradigm based on two-terminal diodes.

ACKNOWLEDGEMENTS

The authors acknowledge the support provided by the State Key Program for Basic Research of China (2013CB632705, 2011CB922004), the National Natural Science Foundation of China (10990104, 11334008, and 61290301), the Fund of Shanghai Science and Technology Foundation (13JC1408800).

MATERIALS AND METHODS

Finite element calculation is performed by means of the commercial soft-package 'Sdevice' by Synopsys Inc[35]. The graphene layer has been modeled as a 3.4 Å thick semi-metallic channel one, as shown in Fig. 1a. The energy dispersion relations and density of state distribution have been fitted to obtained the charge in the graphene with Fermi integral of order 1, $n_{sn}-n_{sp}=en_i(F_1(\phi_{Fn}/k_BT)-F_1(-\phi_{Fh}/k_BT))$, where $F_1(\varepsilon/k_BT)=\int\xi d\xi\ (1+\exp(\xi-\varepsilon/k_BT))^{-1}$ with $\varepsilon=\phi_{n,p}$ being difference between the quasi-Fermi level and Dirac point, and $n_i\sim1\times10^{11}cm^{-2}$ being the intrinsic carrier density at room temperature. In addition, the carriers distribution in the graphene channel is governed by the Poisson equation $\nabla\varepsilon\cdot\nabla\Psi=-q(n_{sp}-n_{sn}+N_D-N_A)$, where Ψ is the channel potential. N_D and N_A represent the impurities, and they lead to the electron-hole traps in graphene[2]. The charge transport in graphene channel is governed by the continuity equations, $\nabla\cdot J_{n,p}=qdn_{sn,sp}/dt$, where $J=J_n+J_p=\mu_n n_{sn}\nabla E_{Fn}+\mu_p n_{sp}\nabla E_{Fp}$ is the current density, and $\mu_{n,p}$ is the electron/hole mobility, and $E_{Fn,p}$ is the quasi-Fermi level along the channel. Monte Carlo simulations have suggested that the drift velocity exhibit slow saturation behavior at high electric field as follows[22,29,30],

$$\mu(E_x)=\frac{\mu_0}{[1+(\mu_0|E_x|/v_{sat})]}$$

where μ_0 is the low-field mobility limited by the charged impurity scattering (in our works, low field mobility follows the fitting of Ref. 36), E_x is the channel electric field along the current direction, and v_{sat} is the saturation velocity strongly depend on the surface polar optical phonon scattering[16]. Here, $v_{sat}=v_F(\hbar\omega_{OP}/E_F)\sim\omega_{OP}/(\pi n_s)^{0.5}$, and $\hbar\omega_{OP}$ is 55meV for SiO_2, 87meV for Al_2O_3. The sheet density at the drain end can be simplified as $n_s(x)=C_d(V_{gs}\text{-}V(x))$, $V(x)$ is the voltage drop

at the drain end, the regime of NDC is determined by the relation (i. e. $dv/v_0<dn/n_0$), and x is opposite to the current direction:

$(V_{gs}-V(x))\cdot(1+\mu_0 E_x/v_{sat})(1+\mu_0|dV(x)/dx|/v_{sat})^{-1}+dV(x)/dE_x\cdot E_x<0$ for electric field $E_x<0$, **condition 1,**

$(V_{gs}-V(x))\cdot(1+\mu_0|dV(x)/dx|/v_{sat})^{-1}+dV(x)/dE_x\cdot E_x<0$ for electric field $E_x>0$, **condition 2.**

In the left hand side of conditions 1 and 2, the second term is strongly related to the effect of contact-induced doping (seeing Fig. 2e), and $dV(x)/dE_x\cdot E_x>(<)0$ corresponds to the electron (hole) dominating the channel. In the electronic dominated GFET (in our cases, as shown Fig. 1a), the condition 1 can be satisfied in the channel by sweeping the drain bias V_{ds}, and then, the electric $|E_x|$ can be increased, Finally, the NDC effect is caused. If the voltage drop across the channel is increased further, the value of the second term in the left hand side of condition 1 can exceed the first one, and the current recovers to the sublinear regime. In contrast, the condition 2 can not be satisfied at the drain end for all bias voltage range. When the device enters into the NDC regime, the junction resistance $R_{JS,D}$ changes (seeing the text) in order to maintain the voltage drop across the channel, and the second term should increase until the junction resistance at the drain side R_{JD} is sufficient low. The judgment conditions can also be applied for the hole-dominated transport regime, but it should be noted that the two terms at the left side of the inequality should reverse their signs. By considering the doping effect induced with the contact, the electric field E_x changes its direction around the flat-band point (seeing Fig. 2), and the condition 1 can be satisfied at the left side of the point. In addition, it is interesting to see that the NDC regime depends strongly on the saturation velocity v_{sat}, low-field mobility, and doping density at graphene electrodes. Thus, it is indicated that the NDC effect can be optimized during the designing and fabrication of graphene-based NDC devices.

REFERENCES AND NOTES

[1]Novoselov, K. S.; Geim, A. K.; Morozov, S. V.; Jiang, D.; Zhang, Y.; Dubonos, S. V.; Grigorieva, I. V.; Firsov, A. A. Electric Filed Effect in Atomically Thin Carbon Films. Science **2004**, 306,666-669.

[2]Geim, A. K.; Novoselov, K. S. The Rise of Graphene. Nature Materials **2007**, 6, 183-191.

[3]Bao, Q.; Loh, K. P. Graphene Photonics, Plasmonics, and Broadband Optoelectronic Devices. ACS nano **2012**, 6, 3677-3694.

[4]Grigorenko, A. N.; Polini M.; Novoselov, K. S. Graphene Plasmonics. Nature photonics **2012**, 6, 749-757.

[5]Liao, L.; Bai, J.; Qu, Y.; Lin, Y.; Li, Y.; Huang, Y.; Duan, X. High-κ Oxide Nanoribbons as Gate Dielectrics for High Mobility Top-Gated Graphene Transistors. Proc Natl Acad Sci USA. **2010**, 13, 6711-6715.

[6]Cheng, R.; Bai, J.; Liao, L.; Zhou, H.; Chen, Y.; Liu, L.; Lin, Y.; Jiang, S.; Huang, Y.; Duan, X. High-Frequency Self-Aligned Graphene Transistors with Transferred Gate Stacks. Proc Natl Acad Sci USA. **2012**, 109, 11588-11592.

[7]Britnell, L.; Ribeiro R. M.; Eckmann A.; Jalil R.; Belle B. D.; Mishchenko A.; Kim Y. -J.; Gorbachev, R. V.; Georgiou, T.; Morozov, S. V.; Grigorenko, A. N.; Geim, A. K.; Casiraghi, C.; Castro Neto, A. H.; Novoselov, K. S. Strong Light-Matter Interactions in Heterostructures of Atomically Thin Films. Sciencexpress **2013**, 340, 1311-1314.

[8] Orlita, M.; Faugeras, C.; Plochocka, P.; Neugebauer, Martinez, G.; Maude, D. K.; Barra, A.-L.;

Sprinkle, M.; Berger, C.; de Heer, W. A. and Potemski, M. Approaching the Dirac Point in High-Mobility Multilayer Epitaxial Graphene. Phys. Rev. Lett. **2008**, 101, 267601.
[9] Lin, Y.-M.; Dimitrakopoulos, C.; Jenkins, K. A.; Farmer, D. B.; Chiu, H. –Y.; Grill, A.; Avouris, Ph. 100-GHz Transistors from Wafer-Scale Epitaxial Graphene. Science. **2010**, 327, 662.
[10]Schwierz, F. Graphene transistors. Nature nanotechnology. **2010**, 5, 487.
[11]Wu, Y.; Jenkins, K. A.; Valdes-Garcia, A.; Farmer, D. B.; Zhu, Y.; Bol, A. A.; Dimitrakopoulos, C.; Zhu, W.; Xia, F.; Avouris, P. and Lin, Y. State-of-the Art Graphene High-Frequency Electronics. Nano Letters. **2012**, 12, 3062-3067.
[12]Zheng, J.; Wang, L.; Quhe, R.; Liu, Q.; Li, H.; Yu, D.; Mei, W.; Shi, J.; Gao, Z.; Lu, J. Sub-10nm Gate Length Graphene Transistors: Operating at Terahertz Frequencies with Current Saturation. Scientific Reports. **2012**, 3, 1314.
[13]Liao, L.; Bai, J.; Cheng, R.; Lin, Y.; Jiang, S.; Qu, Y.; Huang, Y.; Duan, X. Sub-100nm Channel Length Graphene Transistors. Nano Letters. **2010**, 10, 3952-3956.
[14]Szafranek, B. N.; Fiori, G.; Schall, D.; Neumaier, D.; Kurz, H. Current Saturation and Voltage Gain in Bilayer Graphene Field Effect Tansistors. Nano Letters. **2012**, 12, 1324-1328.
[15]Zhuang, Y.; Tang, T.; Girit, C.; Hao, Zhao; Martin, M. C.; Zettl, A.; Crommie, M. F., Shen, Y. Ron; Wang, F. Direct observation of a widely tunable bandgap in bilayer graphene. Nature. **2009**, 459, 820-823.
[16] Meric, I.; Han, M. Y.; Yong, A. F.; Ozyilmaz, B.; Kim, P.; Shepard, K. L. Current saturation in zero-bandgap, top-gated graphene field-effect transistors. Nature nanotechnology. **2008**, 3. 654-659.
[17] Meric, I.; Dean, C. R.; Young, A. F.; Baklitskaya, N.; Tremblay, N. J.; Nuckolls, C.; Kim, P.; Shepard, K. L. Channel Length Scaling in Graphene Field-Effect Transistors Studies with Pulsed Current-Voltage Measurements. Nano Letters. **2011**, 11, 1093-1097.
[18] Han, S.; Reddy, D.: Carpenter, G. D.; Franklin, A. D.; Jenkins, K. A. Current Saturation in Sub-micrometer Graphene Transistors with Thin Gate Dielectric: Experiment, Simulation, and Theory. ACS nano. **2012**, 6, 5220-5226.
[19]Wu, Y.; Farmer, D. B.; Zhu, W.; Han, S.; Dimitrakopoulos, C. D.; Bol, A. A.; Avouris, P.; Lin, Y. Three-Terminal Graphene Negative Differential Resistance Devices. ACS nano. **2012**, 6, 2610-2616.
[20]Majumdar, K.; Kallatt, S.; Bhat, N. High field carrier transport in graphene: Insights from fast current transient. Appl. Phys. Lett. **2012**, 101, 123505.
[21]Barreiro, A.; Lazzeri, M.; Moser, J.; Mauri, F.; Bachtold, A. Transport Properties of Graphene in the High-Current Limit. Phys. Rev. Lett. **2009**, 103, 076601.
[22]Perebeinos, V.; Avouris, P. Inelastic scattering and current saturation in graphene. Phys. Rev. B. **2010**, 81, 195442.
[23]Bai, J.; Liao, L.; Zhou, H.; Cheng, R.; Liu, L.; Huang, Y.; Duan, X. Top-Gated Chemical Vapor Deposition Grown Graphene Transistors with Current Saturation. Nano Letters. **2011**, 11, 2555-2559.
[24]Giovannetti, G.; Khomyakov, P. A.; Brocks, G.; Karpan, V. M.; van den Brink, J.; Kelly, P. J. Doping Graphene with Metal Contacts. Phys. Rev. Lett. **2008**, 101, 026803.
[25]Song, S. M.; Park, J. K.; Sul, O. J.; Cho, B. J. Nano Letters. **2012**, 12, 3887-3892.
[26]Xia, F.; Perebeinos, V.; Lin, Y., Wu, Y.; Avouris, P. The origins and limits of metal-graphene junction resistance. Nature nanotechnology. **2011**, 6, 179-184.

[27]Farmer, D. B.; Golizadeh-Mojarad, R.; Perebeinos, V.; Lin, Y.; Tulevski, G. S.; Tsang, J. C.; Avouris, P. Chemical Doping and Electron-Hole Conduction Asymmetry in Graphene Devices. Nano Letters. **2009**, 6, 388-392.

[28]Alarcón, A.; Nguyem, V.; Berrada, S.; Querlioz, D.; Saint-Martin, J.; Bournel, A.; Dollfus, P. Pseudosaturation and Negative Differential Conductance in Graphene Field-Effect Transistors. IEEE Tran. Electron Devices. **2013**, 60, 985-991.

[29]Wang, X.; Xu, H.; Min, J.; Peng, L.; Xu, J. Carrier sheet density constrained anomalous current saturation of graphene field-effect transistors:kink and negative differential resistances. Nanoscale. **2013**, 5, 2811-2817.

[30]Chauhan, J.; Guo, J. High-Field Transport and Velocity Saturation in Graphene. Appl. Phys. Lett. **2009**, 95, 023120.

[31]Sonin, E. B. Effect of Klein tunneling on conductance and shot noise in ballistic graphene. Phys. Rev. B. **2009**, 79, 195438.

[32]Thornber, K. K. J. Appl. Phys. **1980**, 51, 2127.

[33]Perebeinos, V.; Avouris, P. Inelastic Scattering and Current Saturation in Graphene. Phys. Rev. B. **2010**, 81, 195442.

[34]Wang, S. Q.; Mahan, G. D. Electron Scattering from Surface Excitation. Phys. Rev. B. **1972**, 6, 4517-4524.

[35] Sdevice, Sentaurus-TCAD Mannual, Version D-2010. 03, Synopsys.

[36]Zhu, W.; Perebeinos, V.; Freitag, M.; Avouris, P. Carrier Scattering, Mobilities, and Electrostatic Potential in Monolayer, Bilayer, and Trilayer Graphene. Phys. Rev. B. **2009**, 80, 235402.

Lin Wang received the B. S. degree in Applied Physics (with honors) from Zhejiang University of Science and Technology, Hangzhou, China, in 2008, and the Ph. D. degree in Microelectronics and Solid-State electronics (with honors) from Shanghai Institute of Technical Physics, Chinese Academy of Sciences, Shanghai, China, in 2013. He has been awarded special prize of president scholarship for distinguished postgraduate student. He is currently a Research Assistant in Shanghai Institute of Technology Physics, Chinese Academy of Sciences. He has authored or coauthored more than 20 technical journal papers and conference presentations.

His current research interests include plasma wave detection of terahertz radiation using graphene and GaN, simulation and modeling of carbon-based nanomaterials and devices, graphene-like optoelectronics. Email: wanglin@mail.sitp.ac.cn.

Xiaoshuang Chen received the Ph. D. degree in Condensed Matter physics from Nanjing University, Jiangsu, China in 1995. He has been a research fellow in Korea Institute of Advanced Study, University of Tokyo, Japan, and Humboldt research fellow in Universität Würzburg, Germany. He has also coauthored more than 100 publications. He is a Professor in Shanghai Institute of Technology Physics, the vice Director of National Laboratory for Infrared Physics, and won many national prizes for solving problems in infrared electronics.

His current research interests include low-dimensional field-effect transistor (FET) terahertz detectors, the physics of nano-electronic device and photonic crystal, first principle of infrared photo-electronic material and device. (Email: xschen@mail.sitp.ac.cn; Tel: +86-21-2505 1403, Fax: +86-21-6583 0734).

Yibin Hu received the Ph.D. degree from Institute of Physics Chinese Academy of Sciences in 2007. In 2013, he joined Shanghai Institute of Technical Physics Chinese Academy of Sciences.

He is familiar with the first principles quantum transport modeling which is based on density functional theory and Keldysh nonequilibrium Green's function method. His previous works include studies of molecular tunneling junctions, tunneling magnetoresistance devices and topological insulator materials. His current research interests are centered on the physics of quantum transport of nanoscale transistors.

Anqi Yu received the B.S. degree in microelectronics from Jiaotong University, Shanghai, China, in 2010. He is currently working toward the Ph.D. degree in microelectronics and solid-state electronics at the Shanghai Institute of Technical Physics, Chinese Academy of Sciences, Shanghai, China.

His current research interests include graphene-plasmon-based terahertz wave detection and modulation.

Wei Lu received B. S. degree in physics from Fudan University, Shanghai, China, in 1983, and the Ph. D. degree in from Shanghai Institute of Technology Physics in 1988. He has been the research fellow in Technical University of Braunschweig, Germany, 1989, and visiting professor in many countries. He is currently a Professor in Shanghai Institute of Technology Physics, the Director of National Laboratory for Infrared Physics and Shanghai Physical Society. He has authored or coauthored more than 150 publications on Optoelectronic Materials and Devices and won many National Awards. He is also serving on the editorial board of the journal "*Journal of Applied Physics*".

His current research interests include HgCdTe-based photodetectors, Semiconductor Physics and Solid Spectroscopy, Physics of Condensed Matter.